Comparison of shot encoding functions for reverse-time migration

Francesco Perrone and Paul Sava, Center for Wave Phenomena, Colorado School of Mines*

SUMMARY

Reverse-time migration (RTM) represents one of the most accurate, but also one of the costliest algorithms available for imaging in complex media. The RTM computational cost can be reduced by shot encoding, i.e. by imaging simultaneously a large number of shots. This approach reduces computational cost if the number of encoded seismic experiments is smaller than the number of shots. Different encoding strategies are possible, including linear and random encoding which represent end-members of a more general family of encodings. For a fixed maximum delay (i.e., computational cost), we can trade spatial bandwidth for cross-talk noise. Linear encoding is characterized by low bandwidth and high signal-to-noise ratio, while random encoding is characterized by high bandwidth and low signal-to-noise ratio. Mixed encodings allows us to calibrate the amount of resolution desired in the migrated image, given an acceptable level of noise in the image.

INTRODUCTION

Reverse-time migration (RTM) is one of the most computationally expensive algorithm for seismic imaging. The high computational burden is balanced by the ability of this method to deal with multipathing, steep dips, and over-turning and prismatic waves (Gray et al., 2001). In this method, shot and receiver wavefields are respectively forward and backward propagated using the subsurface velocity model. Then, reflectivity is extracted from the reconstructed wavefield through an imaging condition. The cost of wavefield extrapolation is proportional to the time length of the recorded seismic signals.

RTM can be performed by imaging separately seismic experiments recorded in the field (shots). Alternatively, using the linearity of the wave-equation operator, we can image artificial experiments representing combinations of shots. The advantage of imaging with composite shots is that we potentially use fewer migrations to account for all the acquired data (Stork and Kapoor, 2004; Etgen, 2006). The disadvantage of this approach is that the seismic experiments interfere with one-another leading to imaging artifacts.

Different approaches can be taken for shot encoding (Whitmore, 1995; Morton and Ober, 1998; Romero et al., 2000; Sourbaras, 2006; Zhang et al., 2007), among which a popular option is represented by plane-wave migration. In plane-wave migration, the information corresponding to different shots is encoded by delays proportional to the distance relative to a reference in space. The main drawback of plane-wave RTM is that, if we want to achieve high spatial bandwidth, we need to consider large delays over the imaging space. This delay, which could be in the order of seconds for plane-waves with steep angles of incidence, adds significantly to the overall computational cost of the method. Zhang et al. (2007) propose an alternative encoding to alleviate this problem by using the so-called *harmonic source encoding* which is a time-domain version of a frequency domain encoding introduced in (Sourbaras, 2006). The difficulty with implementing this kind of encoding in the time-domain is that it requires convolution with a function that decays like $1/t$, which is not practical as time approaches zero. Furthermore, the overall cost issue remains since the total duration of the encoded experiments depends on the encoding.

In this paper, we compare different types of time-domain encodings and seek to derive parameters that balance the advantages and disadvantages of various options. We consider linear and random encoding as end-members of a family of possible combinations in which we trade between spatial bandwidth and cross-talk. An optimal solution achieves similar spatial bandwidth and signal-to-noise ratio as shot record migration, but using a smaller number of experiments and a smaller increase in extrapolation time.

THEORY

Migration with shot encoding consists of imaging a linear superposition of the wavefields corresponding to all the acquired shots. Let us indicate with $s_k(\mathbf{x},t)$ and $r_l(\mathbf{x},t)$ the source and receiver wave-field for the k-th and l-th shot, respectively. Then the composite wavefields can be expressed as

$$S(\mathbf{x},t,\theta) = \sum_k s_k(\mathbf{x},t) * \delta(t - f(\mathbf{x}_k,\theta)) \qquad (1)$$

$$R(\mathbf{x},t,\theta) = \sum_l r_l(\mathbf{x},t) * \delta(t - f(\mathbf{x}_l,\theta)), \qquad (2)$$

where $f(\mathbf{x}_k,\theta)$ represents the delay applied to the k-th shot wave-fields as a function of the shot position $\mathbf{x}_k$ and the parameter θ. The parameter θ spans the encoding axis. For example, in the case of plane-wave migration (Whitmore, 1995), we have $f(\mathbf{x}_k,\theta) = \frac{\sin(\alpha\theta)}{v}(\mathbf{x}_k - \mathbf{x}_0)$ where $\mathbf{x}_0$ is a reference point and $\alpha\theta$ represents the take-off angle of a single plane-wave. If N represents the total number of shots and M the number of different encodings, this strategy is effective if $M < N$, that is we can obtain an image which is comparable in quality to shot-record migration (SRM) with a smaller number of migrations.

The main issue in implementing this approach is related to spurious events that are present in the final result and depend essentially on the imaging condition applied to the wave-fields. The standard imaging condition extracts an image by computing the zero-lag cross-correlation of the source and receiver wave-fields extrapolated in the background velocity model, and the complete image is obtained by stacking the partial images for the different shots. In the case of shot-encoding migration (SEM), the image is given by the following expression:

$$I(\mathbf{x}) = \sum_\theta \sum_t S(\mathbf{x},t,\theta) R(\mathbf{x},t,\theta) \qquad (3)$$

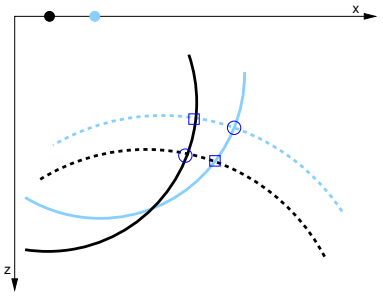

Figure 1: Artifacts generated by the imaging condition: the wave-fields corresponding to different shots are represented with different colors. The source and receiver wave-fields are represented by solid and dashed lines, respectively. The correct image is produced at the points indicated by the circles, the squares highlight cross-talk.

Plugging equations 1 and 2 into equation 3 and transforming to the Fourier domain we obtain

$$I(\mathbf{x}) = \sum_{\omega}\sum_{k}\sum_{l} s_k(\mathbf{x},\omega) r_l^*(\mathbf{x},\omega) \sum_{\theta} e^{i\omega[f(\mathbf{x}_l,\theta)-f(\mathbf{x}_k,\theta)]}. \tag{4}$$

Analyzing equation 4, we can observe that the signal involves a single summation ($k=l$), while the artifacts accumulate contribution from a double summation ($k\neq l$). Therefore, the artifact level in the image after a single encoding is overwhelming and several encodings are needed to attenuate the cross-talk.

Equation 4 points out the equivalence condition between SEM and SRM. In order to decouple the wave-fields for different experiments, we need to insure that

$$W(\theta) = \sum_{\theta} e^{i\omega[f(\mathbf{x}_l,\theta)-f(\mathbf{x}_k,\theta)]} \approx \delta_{kl}, \tag{5}$$

where δ_{kl} is the Kronecker symbol. Plane-wave migration satisfies condition 5 given that a large number of θ values are used (Liu et al., 2006), although the number of plane-waves we need to migrate depends on the complexity of the model and its spatial spectrum. Using an insufficient number of plane-waves, we do not comply with the cross-talk condition given by equation 5 and the image experiences both poor spatial resolution and incomplete cross-talk cancellation.

A different strategy for attenuating the artifacts is offered by random-phase encoding (Morton and Ober, 1998). The combination of all the shots randomly delayed in time produces randomly distributed artifacts that stack out by summation along the axis representing the realization of random delays applied to the recorded data. The attenuation of cross-talk artifacts is proportional to the number of synthetic migrated experiments (Romero et al., 2000). Random-phase encoding allows imaging a large number of components of the spatial spectrum.

In this work, we consider three shot-encoding migration schemes in the framework of RTM: linear (L-SEM), random (R-SEM) and a combination of the two (M-SEM). The cross-talk function $W(\theta)$ for the three encodings are

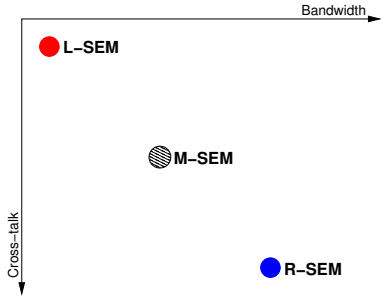

Figure 2: Bandwidth vs. cross-talk for different types of shot encoding.

$$W_L(\theta) = \sum_{\theta} e^{i\omega\frac{\sin(\alpha\theta)}{v}[\mathbf{x}_l-\mathbf{x}_k]}, \tag{6}$$

$$W_R(\theta) = \sum_{\theta} e^{i\omega[t_{l,\theta}-t_{k,\theta}]}, \tag{7}$$

$$W_M(\theta) = \sum_{\theta} e^{i\omega\left[\frac{\sin(\alpha\theta)}{v}(\mathbf{x}_l-\mathbf{x}_k)+(t_{l,\theta}-t_{k,\theta})\right]}. \tag{8}$$

These functions depend on both θ and the pairs $(\mathbf{x}_k,\mathbf{x}_l)$. Notice that in all three cases, if $\mathbf{x}_k=\mathbf{x}_l$ then $W(\theta)$ accumulates contributions for each value of θ. Nonetheless, the off-diagonal behavior is different for the three encodings. $W_L(\theta)$ is the discrete counterpart of the Fourier transform of a boxcar function and it is the superposition of shifted replicas of a sinc function. If the range of take-off angles is even with respect to $\theta=0$, and the sampling of the θ axis is appropriate, then the summation gives a zero-phase function with side-lobes that decrease as $1/(\mathbf{x}_k-\mathbf{x}_l)$. This behavior of the side-lobes of the cross-talk function explains the low level of artifacts in the final image. However, the spatial bandwidth is constrained by the width of the main lobe of $W(\theta)$, which depends on the range of take-off angles. On the other hand, R-SEM allows recovery of all the possible spatial components, since we can rewrite equation 7 as

$$\sum_{\theta} e^{i\omega[t_{l,\theta}-t_{k,\theta}]} = M\delta_{kl} + \sum_{\theta,k\neq l} e^{i\omega[t_{l,\theta}-t_{k,\theta}]}. \tag{9}$$

The quantity $e^{i\omega[t_{l,\theta}-t_{k,\theta}]}$ is a random vector and if its phase is uniformly distributed on the unit circle, then the stack along the θ axis attenuates the noise level by a factor $1/M$. Notice, however, that the cross-talk contribution is almost flat as a function of the distance $(\mathbf{x}_k-\mathbf{x}_l)$ while it is decreasing as the inverse of this distance for L-SEM. The above considerations suggest the cartoon in Figure 2. We can trade between cross-talk and spatial bandwidth by combining linear- and R-SEM. This goal is achieved by an encoding function which is the superposition of a linear trend and a random sequence. If we rewrite equation 8 as

$$\sum_{\theta} e^{i\omega[p_\theta(\mathbf{x}_l-\mathbf{x}_k)+(t_{l,\theta}-t_{k,\theta})]} = M\delta_{kl} + \sum_{\theta,k\neq l} e^{i\omega[p_\theta(\mathbf{x}_l-\mathbf{x}_k)+(t_{l,\theta}-t_{k,\theta})]}, \tag{10}$$

we can observe a δ function for $k=l$, which is associated with the signal and the off-diagonal cross-talk term for $k\neq l$.

The goal is to control the artifact level using the decay of the side-lobes of the function given by equation 6 and, at the same time, to narrow the width of the main lobe, thus gaining spatial bandwidth using the random perturbation.

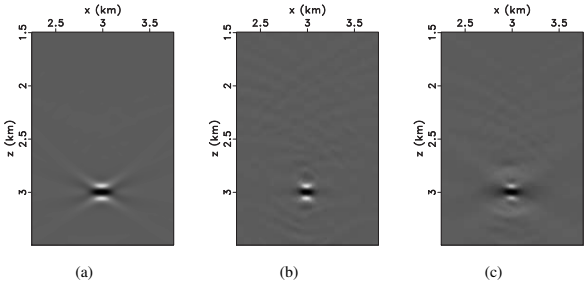

Figure 3: Images of a point scatterer in a constant medium obtained by (a) L-SEM, (b) R-SEM, and (c) M-SEM.

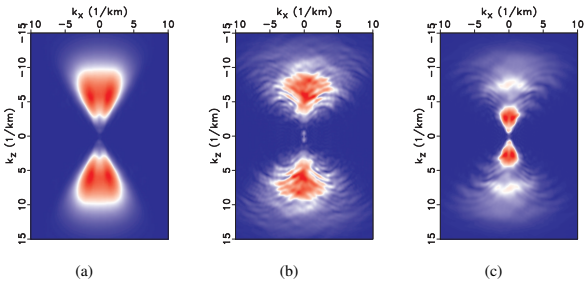

Figure 4: Amplitude spectra of the point scatterer images shown in Figures 3(a)-3(c).

EXAMPLES

We first illustrate our method with a point scatterer in a constant velocity background. We compare the images obtained by stacking 20 experiments constructed with linear, random and mixed encoding. Figures 3(a)-3(c) show the results obtained by L-SEM, R-SEM and M-SEM, respectively. In all three cases the maximum delay applied to wave-fields is the same and equal to 1 s. The fixed maximum delay insures that all migrations have the same cost regardless of the encoding type. In our examples, we compare the quality of the migrated images at a fixed cost. Notice the lower focusing of the image obtained by L-SEM. The point is spread in the horizontal direction because in the imaging process we have not used plane-waves with high values of θ. On the other hand, the image is clean because the shots cross-talk decreases quickly with the distance $(\mathbf{x}_k - \mathbf{x}_l)$. Figure 3(b) represents the other extreme in the trade-off between cross-talk and spatial bandwidth. In this case, a wider range of the spatial components is imaged but cross-talk noise is also present in the image.

The stack of the different experiments is effective for this simple model but the result rapidly worsens with increasing complexity of the model. Figure 3(c) shows the image obtained by M-SEM. We can observe a spatial resolution closer to R-SEM but fewer artifacts. The amplitude spectra in Figures 4(a)-4(c) highlight the smaller spatial bandwidth of L-SEM with respect to both R-SEM and M-SEM. Nonetheless, they show the distortion of the spectrum, i.e., the artifacts are still present in the image but with a smaller magnitude relative to imaging with R-SEM.

The cross-talk in the final image is heavily dependent on the model complexity. In a complicated velocity model, plane-waves get distorted and the phase relations that define $W_L(\theta)$ break down as soon as inhomogeneities are encountered. However, R-SEM is more robust against this kind of problem since there is no phase coherency to be destroyed. Let us consider the complex Sigsbee model. Again, the computational cost is fixed. We consider 50 shots for SRM and 50 different experiments that combine all 500 shots for the other three strategies.The migration algorithm used is RTM and the maximum delayed applied to a single shot is ± 2 s.

Figure 5 shows the image obtained by migrating 50 shots separately. In order to compare the different encoding strategies, we look at the part of the image indicated by the box, under the tip of the salt body. This area suffers from illumination problems for L-SEM since the synthetic plane-waves are severely distorted by the salt. We can observe poorer spatial resolution in Figure 6(b) with respect to 6(a). The number of plane-wave components used is clearly insufficient for the complexity of the Sigsbee model. R-SEM recovers a more complete image where the illumination is high but loses coherency under the salt body because of the overwhelming level of the cross-talk. On the other hand, M-SEM allows recovery of most of the image spatial bandwidth (in contrast to L-SEM) and controls the cross-talk (in contrast with R-SEM). In Figure 6(d), the sediments under the salt body are more interpretable than in Figure 6(a); the point scatterers are better imaged, and the residual diffractions in Figure 6(a), due to under-sampling of the shot dimension, are attenuated.

CONCLUSIONS

We compare linear and random shot-encoding analyzing their behavior relative to spatial bandwidth and cross-talk artifacts. Combinations of linear and random encodings are effective at increasing spatial bandwith and achieve spatial resolution comparable to that of shot-record migration, while reducing cross-talk artifacts relative to conventional random shot-encoding. Our shot-encoding strategy reduces the overall cost of reverse-time migration for specified spatial bandwidth and signal-to-noise ratio.

ACKNOWLEDGMENTS

We would like to acknowledge the financial support provided by a research grant from Eni E&P, and stimulating technical discussions with Clara Andreoletti and Nicola Bienati.

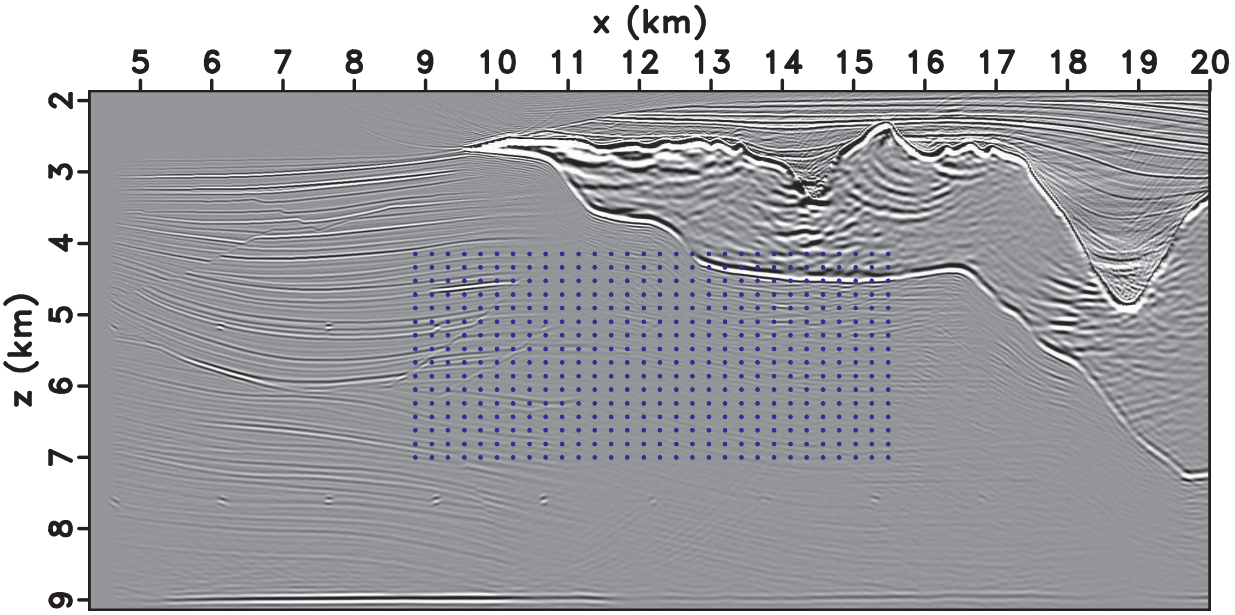

Figure 5: Sigsbee model: shot-record migration of 50 shots. The box highlights the part of the image compared in Figures 6(a)-6(d).

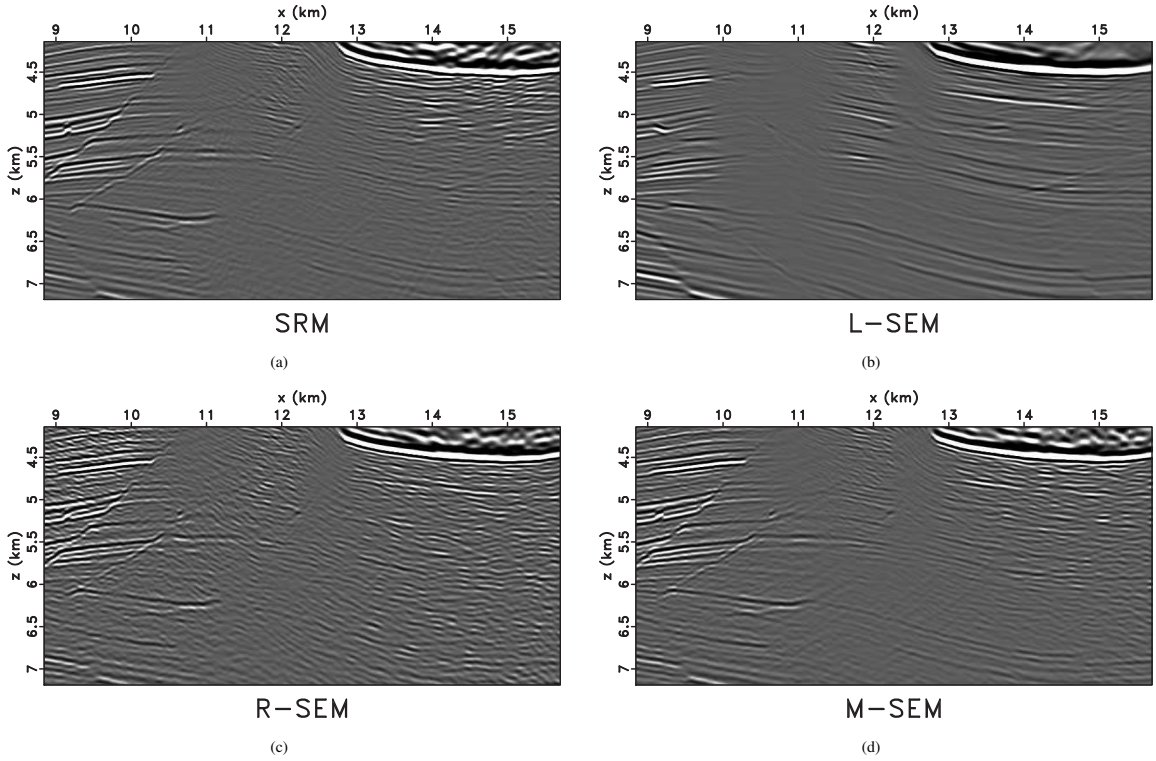

Figure 6: Sigsbee model: detail of the image obtained by SRM, L-SEM, R-SEM and M-SEM.